Three-dimensional metallo-dielectric photonic crystals with cubic symmetry as stacks of two-dimensional screens

J. Shah, K. D. Möller, and H. Grebel

Electronic Imaging Center and the Department of Electrical and Computer Engineering, New Jersey Institute of Technology, Newark, New Jersey 07102

O. Sternberg

NRC–Naval Research Laboratory, Washington, D.C. 20375

J. M. Tobias

U.S. Army Communications-Electronics Command, Fort Monmouth, New Jersey 07703

Received April 23, 2004; revised manuscript received July 30, 2004; accepted August 31, 2004

Metallo-dielectric photonic crystals with cubic symmetries have been studied here both experimentally and theoretically in the millimeter wavelength region (15–60 mm). In a direct analogy to linear systems, we considered the three-dimensional lattices as a stack of two-dimensional resonating screens. The overall three-dimensional structure was introduced in the calculation through a structural phase. Such an approach proved useful in understanding the related mode propagation and guided us in a study of the transition between cubic and centered body cubic symmetries. © 2005 Optical Society of America

OCIS codes: 260.3060; 290.3770.

1. INTRODUCTION

Metallo-dielectric photonic crystals have captured the attention of researchers for filtering and imaging applications.[1–5] The complex characteristic of the corresponding wave propagation[6] has led researchers to investigate simpler three-dimensional forms composed of stacks of inductive two-dimensional screens, where inductive screens are simply metallic screens with holes.[7–9] Such an approach has a direct root in linear filter systems in which the peak resonance wavelength depends on the geometrical dimension and arrangement of the holes.[10] Our interest is in the long-wavelength regime, where the features are smaller than the propagating wavelength. In such a regime, diffraction is limited to only the zero and first order,[5] and thus we may interpret the experimental data by analysis of the (transverse) resonance of a single screen in addition to the obvious resonance in the longitudinal direction (the Bragg condition along the direction of propagation). To account for the screen thickness and the original three-dimensional structure, we introduce additional structural phases.

In general, metallic screens are classified according to their fundamental conduction properties. Inductive screens are metal foils with openings, while patches of metal surrounded by a dielectric matrix are called capacitive screens. These screens have complementary structures, and, if very thin, possess complementary transmission characteristics as well.[11] Computational programs such as the Fourier modal method[12] have demonstrated the validity of the Drude model from the long-wavelength region down to $\lambda = 1\ \mu$m Yet it has been shown by others and us,[13,14] that the long-wavelength characteristics may be extended, in fact, down to nanostructures, or just below the plasma frequency. In this paper we adopt the approach developed for inductive screens and apply it to capacitive screens to study the wave propagation in cubic photonic crystals, namely, propagation in simple cubic (C), body-centered cubic (BCC), and face-centered cubic (FCC) lattices.

2. EXPERIMENT AND ACCURATE SIMULATIONS

Schematic structures of cubic, body-centered cubic, and face-centered cubic lattices are shown in Fig. 1. In our experiments, metal spheres each with a diameter of $d = 6.35$ mm were arranged in a lattice form with a lattice constant of $a = 20$ mm. The transmitter included a continuous-wave signal source (Hewlett-Packard 8673E signal generator) fed through a standard gain horn (MicroTech HWR112). The receiver was made of an identical gain horn connected to a signal spectrum analyzer (Hewlett-Packard 8563E). A baseline characterization of free space as a function of frequency was used as reference. Metal spheres were affixed to thin microwave-transparent substrates with a refractive index close to unity. Various cubic symmetries were achieved by proper stacking of individual layers. The power transmitted through the center axis of the crystal was measured for each of six successive crystal plane layers and normalized

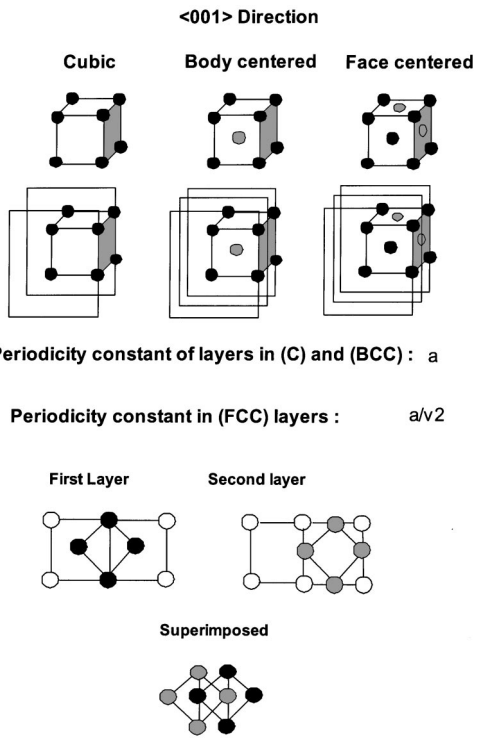

Fig. 1. Schematics of simple cubic (C), body-centered cubic (BCC) and face-centered cubic (FCC) crystal structure. In the body-centered lattice, alternate cubic layers are displaced in the diagonal direction. The distance between the first and the second layer is one half of the lattice constant of the simple cubic structure. The layers of the FCC have periodicity constant of $a/\sqrt{2}$ and separation of $a/2$; alternate layers are shifted by $a/2$.

by the transmission of free space. The experimental transmission spectra for cubic and body-centered cubic structures are shown in Fig. 2 for successive numbers of layers. Previous measurements have been conducted on face-centered cubic structures.[2]

In the simulations, we analyzed a succession of thick, metallo-dielectric capacitive screens. Each layer possesses a resonance wavelength close to the lattice constant a.[14] We used a commercial code[15] to solve the related Maxwell's equations for the stacked screens. Each screen was simulated as a lattice of metallic waveguides with an appropriate cross section. Input data for the program are the lattice constants, the refractive indices of the dielectrics, and the bulk conductivity value of metal sphere. These simulations (Fig. 3) account for all transmission dips in the experimental data shown in Fig. 2. In the following, all simulations were made by using the commercial code[15] unless otherwise noted.

3. MODE ANALYSIS

A. Cubic Lattice and Body-Centered Cubic Lattice

Transmission line theory may be used for interpretation of the various peaks and their dependences on the lattice symmetry (Ref. 14 and Appendix A). Here, we first estimate the resonance wavelength $\lambda^{(R)}$ for a single capacitive screen; see Ref. 16 and the black curve in Fig. 5 below. The screen is then replaced by a filter whose resonance wavelength is $\lambda^{(R)}$. Owing to the periodic construction of screens along the direction of propagation, stacking modes appear. Their corresponding resonance wavelengths $\lambda^{(S)}$ depend on the spacing between screens. This approach is implemented on the experimental data of Fig. 2; the results are shown in Fig. 4. As an example, the resonance wavelength for the stacking mode for a cubic lattice made of metal spheres in air is close to $2s$, twice the distance s between the layers, as one expects from Bragg reflection. Thus we expect an enhanced reflectivity or a dip in the transmission curve.

1. Cubic Lattice

The transverse resonance wavelength $\lambda^{(RC)}$ of a single cubic layer should have a value close to the nearest-neighbor distance $a = 20$ mm and is assigned to the broad peak near $\lambda^{(RC)} = 22$ mm in Fig. 3, estimated from simulation results. The value of the first-order stacking mode $\lambda_1^{(SC)}$ should be close to $2a = 40$ mm, and therefore from Fig. 3 we assign it to the peak at $\lambda_1^{(SC)} = 42$ mm. The second-order stacking mode should appear at $\lambda_2^{(SC)} = 21$ mm and contributes as well to the broad peak at $\lambda = 22$ mm. The third- and fourth-order stacking modes are expected to have values close to $42/m$, where $m = 3$ or 4, and are assigned to the peaks at $\lambda_3^{(SC)} = 16$ and $\lambda_4^{(SC)} = 12$ mm, respectively.

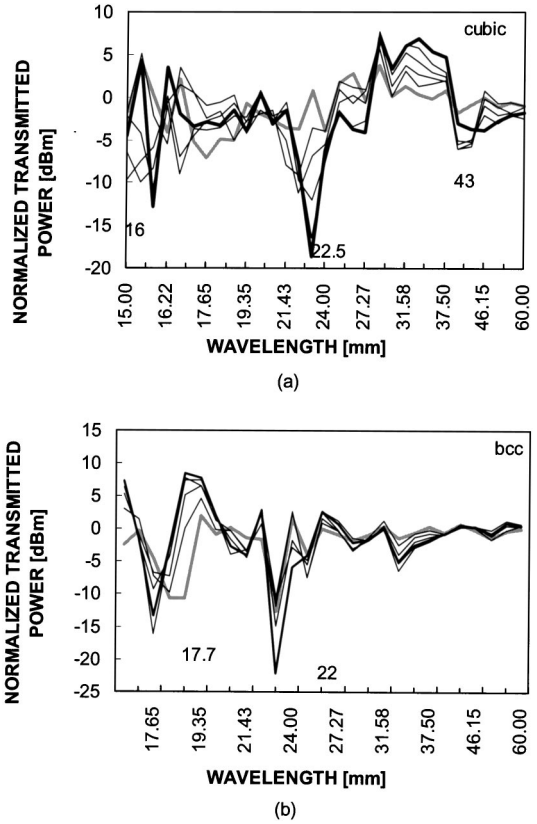

Fig. 2. Experimental transmission power of (a) C and (b) BCC crystals with lattice constant 20 mm and metal sphere diameter $d = 6.35$ mm. The wavelengths in the figures are in millimeters. Successive curves are given for increasing number of layers: gray, one layer; black, five layers.

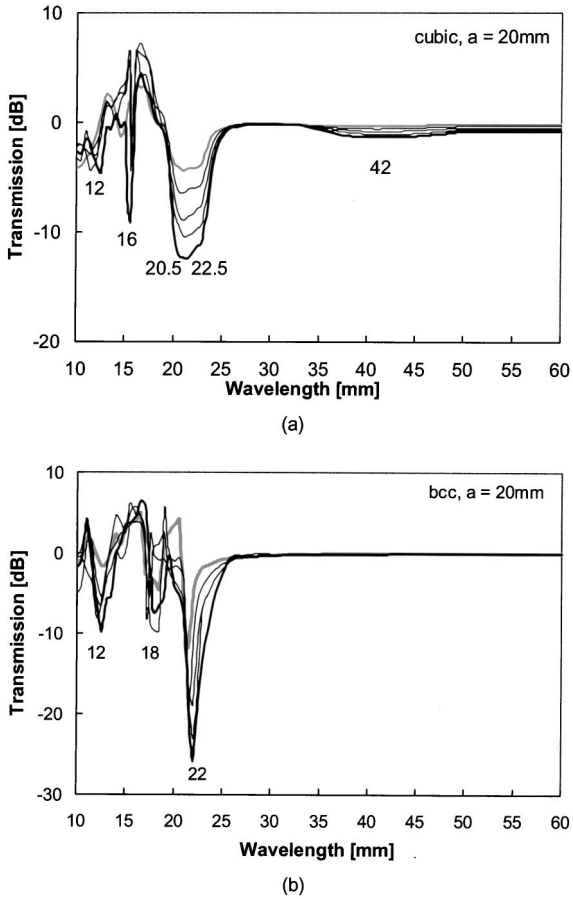

Fig. 3. Simulated transmission of (a) C and (b) BCC structures with lattice constant $a = 20$ mm and metal sphere diameter $d = 6.35$ mm. The wavelengths in the figures are in millimeters. Successive curves are given for increasing number of layers: gray, one layer; black, five layers.

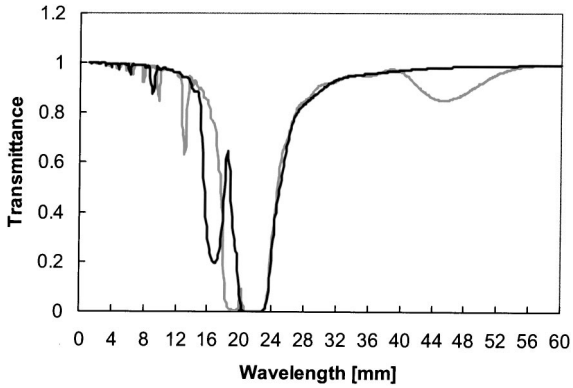

Fig. 4. Simulations produced with transmission line formalism. For cubic structure (gray curve) the input data are periodicity constant $g = 20$ mm, transverse resonance wavelength for each screen $\lambda^{(R)} = 21$ mm, resonance width $\Delta\omega = 0.05$ mm, loss parameter $\alpha = 0.2$, number of layers $f = 6$, spacing between layers $s_1 = 20$ mm, and structure phase $\Phi(\lambda)_{\text{cubic}} = \tan^{-1}[\lambda d/\pi W_{\text{eff}}^2] + c_1$ with $c_1 = \text{const}$. For BCC (black curve), same parameters as for Figs. 2 and 3 with the exception of screen spacing $s_2 = (0.5)s_1 = 10$ mm and a phase constant $\Phi(\lambda)_{\text{BCC}} = \tan^{-1}[\lambda d/\pi W_{\text{eff}}^2] + 2c_1$.

2. Body-Centered Cubic Lattice

Here the lattice constant in the longitudinal direction is only one half of the corresponding value for the cubic lattice. In addition, every other layer is laterally shifted by a half-lattice constant in each direction with respect to its nearest-neighbor layer. Thus, while the resonance wavelength $\lambda^{(\text{RBCC})}$ of a single layer is expected to be $\lambda^{(\text{RBCC})} \sim 20$ mm, this mode is in fact split into two resonance modes. This is because the base structure is composed of two relatively shifted sublayers.[9] One mode is assigned to the peak at $\lambda_1^{(\text{RBCC})} = 18$ mm and the other to the peak at $\lambda_2^{(\text{RBCC})} = 22$ mm. The first-order stacking mode $\lambda^{(\text{SBCC})}$ is assigned to the peak at $\lambda_1^{(\text{SBCC})} = 22$ mm. The second-order stacking mode expected at $\lambda_2^{(\text{SBCC})} \sim 10$ mm is assigned to the peak at $\lambda_2^{(\text{SBCC})} = 12$ mm. A closer look into the simulation is given in Appendix A.

B. Spacing, Sphere Diameter, and Phase Transition

The transmission through up to ten successive 10 screens with transverse lattice constant $a = 15$ mm is shown in Fig. 5. Simulations were made by using the commercial code.[15] A cubic symmetry was assumed for which the

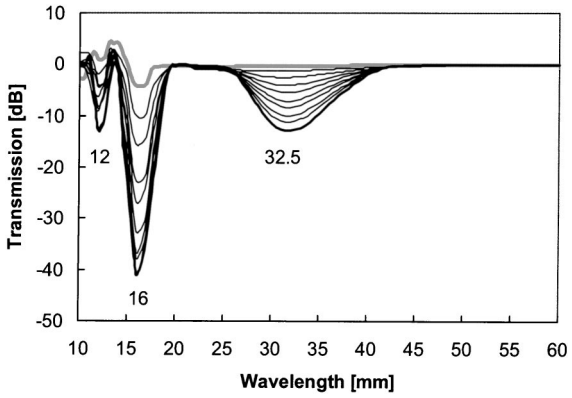

Fig. 5. Simulations of a cubic lattice with $a = 15$ mm. Mode assignment: $\lambda_1^{(\text{RC})} = 16$ mm, $\lambda_1^{(\text{SC})} = 32.5$ mm, $\lambda_2^{(\text{SC})} = 16$ mm, $\lambda_3^{(\text{SC})} = 12$ mm. Note that $\lambda_1^{(\text{RC})}$ overlaps $\lambda_2^{(\text{SC})}$. Shown are layers in succession: gray, one layer; black, ten layers.

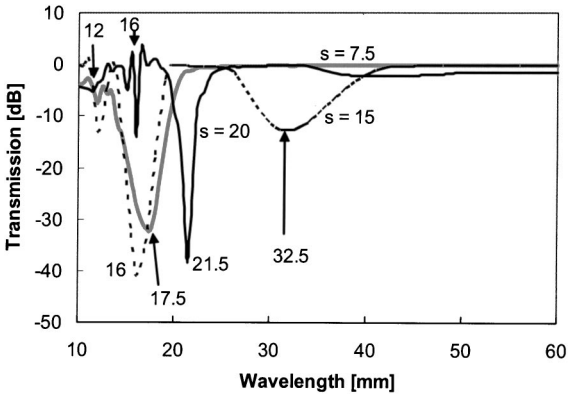

Fig. 6. Cubic lattice with $a = 15$ mm for various separations values, $s = 7.5$ mm, $s = 15$ mm, and $s = 20$ mm, respectively. Mode assignment: dark gray, $s = 7.5$ mm: $\lambda^{(\text{R})} = 17.5$ mm, $\lambda_1^{(\text{S})} = 17.5$ mm. Dotted black: $s = 15$ mm: $\lambda^{(\text{R})} = 16$ mm, $\lambda_1^{(\text{S})} = 32.5$ mm, $\lambda_2^{(\text{S})} = 16$ mm, $\lambda_3^{(\text{S})} = 12$ mm. Black: $s = 20$ mm: $\lambda^{(\text{R})} = 16$ mm, $\lambda_1^{(\text{S})} = 43$ mm, $\lambda_2^{(\text{S})} = 21.5$ mm.

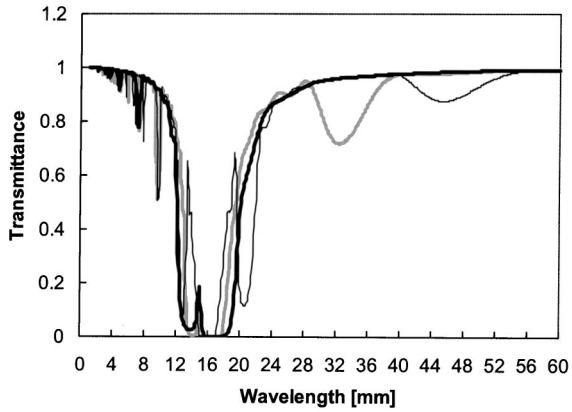

Fig. 7. Transmission line theory calculations for a cubic lattice with $a = 15$ mm for various separation values. Transmission line resonance input: 16 mm. Thick black: $s = 7.5$ mm: $\lambda^{(R)} = 17.5$ mm, $\lambda_1^{(S)} = 17.5$ mm. Gray: $s = 15$ mm: $\lambda^{(R)} = 16$ mm, $\lambda_1^{(S)} = 32.5$ mm, $\lambda_2^{(S)} = 16$ mm, $\lambda_3^{(S)} = 12$ mm. Thin black: $s = 20$ mm: $\lambda^{(R)} = 16$ mm, $\lambda_1^{(S)} = 43$ mm, $\lambda_2^{(S)} = 21.5$ mm.

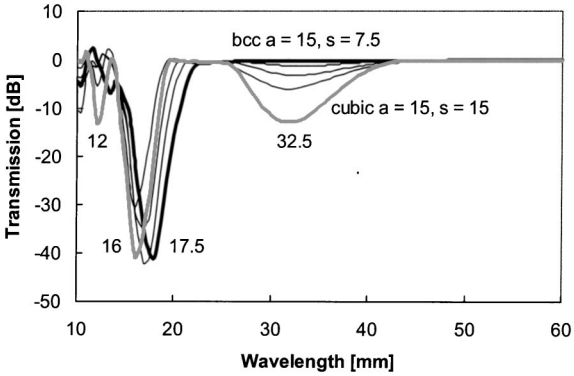

Fig. 8. Transition from BCC (black) to simple C (gray) structure, by decreasing the center sphere's diameter d_b in BCC: $d_b = 6.35$, 5, 4, 1, and 0 mm, respectively. The first-order stacking mode $\lambda_1^{(S)}$ decreases in intensity with decreasing values of d_b. The resonance mode R shifts from $\lambda^{(R)} = 16$ mm to $\lambda^{(R)} = 17.5$ mm.

spacing between layers was $s = 15$ mm. Note that $\lambda_1^{(RC)}$ overlaps $\lambda_2^{(SC)}$. A variation on this theme is shown in Fig. 6. Here we show results for a lattice composed of ten screens, each case at different value, $s = 7.5$, $s = 15$, and $s = 20$ mm. Again, occasional overlapping of transverse resonance and stacking modes occurs at particular screens' spacing. In Fig. 7 we show calculations using transmission line theory. The input transverse resonance wavelength was 16 mm, taken from Fig. 5. The positions of transverse resonance and stacking modes clearly coincide in Figs. 6 and 7.

The layered structure model allows us to study conveniently the phase transitions from BCC to C lattices. The diameter d_b of the center sphere of the BCC lattice may be made increasingly small to approach a zero value while the size of the corner spheres is kept at a value of $d = 6.35$ mm. This transition is shown in Fig. 8. The resonance mode shifts to longer wavelengths, and obviously the stacking mode at $\lambda_1^{(SC)} = 32$ mm disappears for the BCC structure, as mentioned above.

The layered structure model also allows a study of transmission change as a function of the sphere diameter d: We considered a simple cubic lattice with $a = 15$ mm and sphere diameter values of $d = 4$, 6.35, 7.5, and 8 mm (Fig. 9). The fundamental stacking mode appears at $\lambda_1^{(SC)} = 32.5$ mm with increasing intensity for increasing sphere diameter.

C. Face-Centered Cubic Lattice

The structure of the FCC may also be considered as a stack of screens (Fig. 1). Each screen has a lattice parameter of $a/\sqrt{2}$. The separation between screens is $s = a/2$. The transverse resonance mode is expected to peak at $\lambda_1^{(RFCC)} = a/\sqrt{2} \sim 10.6$ mm, and the fundamental stacking mode is expected to peak at $a \sim 15$ mm. The results from simulations for $a = 15$ mm and $d = 6.35$ mm are shown in Fig. 10. Indeed, there appear two peaks at $\lambda_1^{(RFCC)} = 10$ and $\lambda_2^{(SFCC)} = 18$ mm, respectively. The mode near 18 mm has been observed experimentally.[6] The other mode near 10 mm was below the studied wavelength region.

D. Propagation in the ⟨011⟩ and ⟨111⟩ Directions

The layers for a C lattice in the ⟨011⟩ direction are shown schematically in Fig. 11. The layers have rectangular shapes with side length of a and $a\sqrt{2}$. Alternate layers are laterally shifted by $(a/\sqrt{2})$. The separation between

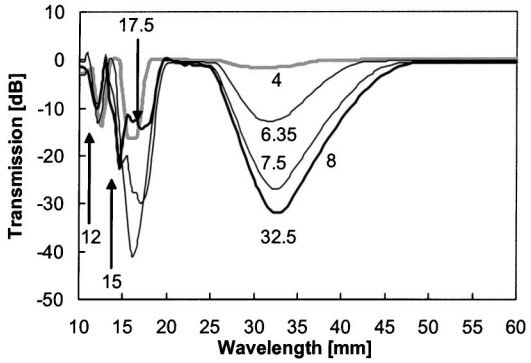

Fig. 9. Cubic lattice with $a = 15$ mm for various values of the ratio d/a of sphere diameter to lattice constant, with $d = 4$, 6.35, 7.5, and 8 mm.

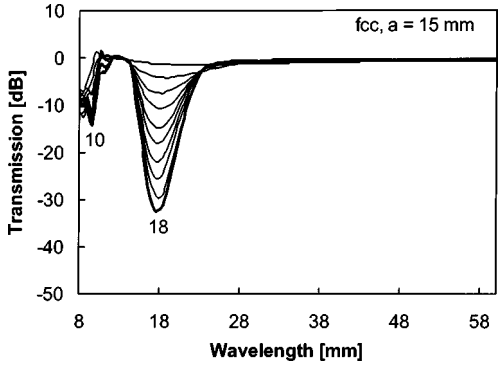

Fig. 10. Simulation for ten layers of a FCC lattice. Note the resonance mode $\lambda^{(RFCC)} = 10$ mm and stacking mode $\lambda^{(SFCC)} = 18$ mm. The peak at 18 mm has been observed experimentally[6] at about the same wavelength.

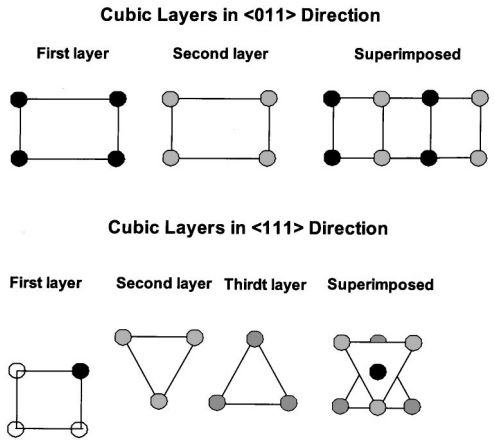

Fig. 11. Schematic of a layered structure of C in the ⟨011⟩ and ⟨111⟩ directions. The layers in the ⟨011⟩ direction have two periodicity constants: a and $a\sqrt{2}$; alternate layers are laterally shifted and spaced apart by $a/\sqrt{2}$. In the ⟨111⟩ direction, the first and fourth layers have cubic structure with periodicity constant a. The second and third layers have hexagonal structure with periodicity constants of $a\sqrt{(3/2)}$ and $a/\sqrt{2}$. The layers are shifted with respect to each other. All layers are separated by $a/\sqrt{3}$.

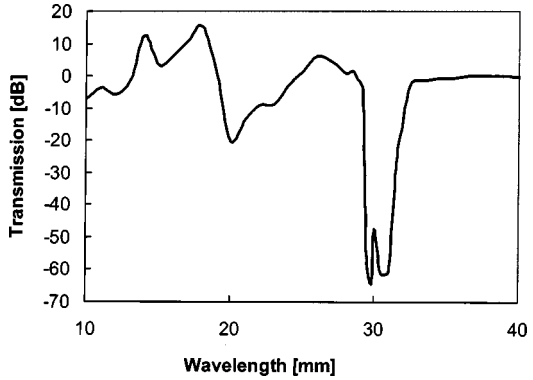

Fig. 12. Propagation in a cubic structure along the ⟨011⟩ direction. The strongest peak is made of two overlapping modes $\lambda_1^{(RC)}$ and $\lambda_1^{(SC)}$ at 30 mm. Weaker peaks are observed at $\lambda_2^{(RC)} = 20$ mm and $\lambda_2^{(SC)} = 15$ mm. The curve is a succession of simulations with 1, 3, 10, and 14 layers.

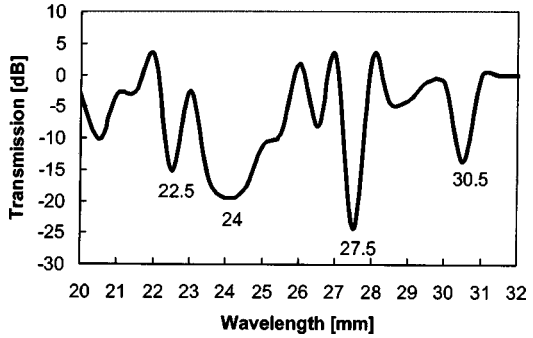

Fig. 13. Propagation in a cubic structure along the ⟨111⟩ direction. The strongest peak is made of two overlapping of hexagonal, $\lambda_1^{(RHX)}$ and stacking, $\lambda_1^{(SC)}$ modes at $\lambda = 24$ mm. The resonance $\lambda_1^{(RC)} = 22.5$ mm is attributed to a cubic screen, whereas the peak at $\lambda_2^{(RHX)} = 30.5$ mm is attributed to a hexagonal screen. The peak at $\lambda = 27.5$ is generated by shifting the hexagonal layers with respect to each other.

layers was taken as $s = a/\sqrt{2}$. The results from the simulation[15] are shown in Fig. 12. Transverse resonance peaks are expected at $\lambda_1^{(RC)} \sim a = 20$ mm and $\lambda_2^{(RC)} \sim a\sqrt{2} = 30$ mm. The first-order stacking modes appears at $\lambda_1^{(SC)} \sim 2a/\sqrt{2} = 30$ mm.

The layers for a C lattice in the ⟨111⟩ direction are shown schematically in Fig. 11. The first and fourth layers have a square-shaped structure with side length of a; thus $\lambda_1^{(RC)} \sim 20$ mm. The second and third layers have hexagonal structures with two transverse resonances at $a\sqrt{(3/2)} = 24$ mm and $(a/\sqrt{2}) = 30$ mm, respectively. These two layers are shifted with respect to each another. All layers are separated by $a/\sqrt{3} = 12$ mm, and the stacking mode (S) is expected at 24 mm. The results from simulation[15] are shown in Fig. 13. The strongest peak is made of two overlapping hexagonal, $\lambda_1^{(RHX)}$, and stacking, $\lambda_1^{(SC)}$, modes at $\lambda = 24$ mm. The resonance $\lambda_1^{(RC)} = 22.5$ mm is attributed to a cubic screen, whereas the peak at $\lambda_2^{(RHX)} = 30.5$ mm is attributed to a hexagonal screen. The peak at $\lambda = 27.5$ mm is generated by shifting the hexagonal layers with respect to each other.

4. DISCUSSION AND CONCLUSIONS

In this paper we analyzed wave propagation through successive stacks of thick capacitive screens. The basic idea was that the wave propagation might be represented as a stack of dispersive filters. The corresponding modes were categorized as follows: transverse resonance mode of a single screen and stacking modes between screens (Bragg diffraction modes in the longitudinal direction). The advantage of this interpretation was demonstrated by using two simulation techniques: One technique employed an accurate commercial code[15] that was corroborated by experiments. In the second technique the experimental dips could be accurately generated and interpreted by using transmission line simulations.

We note that we are operating in the long-wavelength regime where the wavelength is larger than any structural feature. For periodic metallic screens, we find that at resonance, the induced-surface-charge-wave vector $\mathbf{k}_p$ obeys the relationship $\mathbf{k}_t + \mathbf{K} + \mathbf{k}_p = 0$; here $\mathbf{k}_t$ is the transverse wave vector of the incident electric field and $\mathbf{K}$ is the wave vector of the screen. At normal angle of incidence, a surface plasmon wave is launched when $\sin(\theta) = \lambda/qa - (\epsilon_d\epsilon_m/\epsilon_d + \epsilon_m)^{1/2} \equiv 0$, where θ is the angle with respect to the normal. Here λ is the propagating wavelength, a is the lattice constant of the screen, q is an integer signifying plasmon waves extending over more than one period,[3] ϵ_d and ϵ_m are the dielectric constants of the dielectric and the metal portions of the screen, respectively, and typically $(\epsilon_d\epsilon_m/\epsilon_d + \epsilon_m)^{1/2} \sim 1$ for a perfect conductor in air. Note that the polarization of the incident wave at normal incidence conditions is parallel to the screen (i.e., a TE wave). Therefore the lowest-order laterally propagating wave (along the metal surface) has to be acoustic.[17] The second-order propagating mode is optical (nonzero frequency at zero wave number). Lateral confinement of the plasmon wave means that $2\mathbf{k}_p = m\mathbf{K}/q$ with m integer. Therefore, when $\mathbf{k}_t = 0$ (or $\theta = 0$), where $\mathbf{k}$ is the wave vector, the transverse reso-

nance wavelength occurs at $\lambda_c \sim a$ if $2 = m/q$. This means that the mode is leaky (i.e., can be radiated to and from the periodic structure).[17] Alternatively, a resonating capacitive screen may be viewed as contributing to two effects: diffraction and lateral confinement. Diffraction dictates that $\mathbf{k}_t' = \mathbf{k} \pm \mathbf{K}$ where $\mathbf{k}_t'$ is the lateral component of the diffracted wave. At normal incidence, $\mathbf{k}$ has no lateral component and $\mathbf{k}_t' = \mathbf{K}$. Lateral confinement dictates that $2\mathbf{k}_t' = m\mathbf{K}$ with $m = 2$ or higher order of diffraction. In a direct analogy to dielectric optical waveguides, the propagation of a mode along the metal screen is dictated by the cladding material (the dielectric surrounding the screen). In our case, refractive index is $n = 1$ and the wave number of the lateral component is $\mathbf{k}_t \sim \mathbf{k}$. The resonance wavelength will also obey $\lambda \sim a$. The difference between an inductive screen and a capacitive screen at resonance is in the way the incident energy is funneled out of the screen. The inductive screen will transmit all the incident energy in a collinear propagation. The capacitive screen, however, will reflect the energy back. Finally, one may observe that the wave propagation in thick screens is like the propagation of an electromagnetic wave in coupled metallic waveguides. The inductive screen has a dielectric core with metal cladding, whereas the capacitive screen is an antiwaveguide of the latter. Since the field is zero within the metal, then at resonance the electric field just beyond the screen may be either symmetric—namely, of the form $\cos(\mathbf{K} \cdot \mathbf{r})$, with $(\mathbf{K} \cdot \mathbf{r})$ being a dot product—or asymmetric, namely, of the form $\sin(\mathbf{K} \cdot \mathbf{r})$, where $\mathbf{r}$ is $\mathbf{r}:(x, y)$. Either mode will have a resonance wavelength at $\lambda \sim a$.

Our more ambitious goal was to analyze three-dimensional metallo-dielectric photonic crystals by using this method. Comparison between the experiments (Fig. 2) and commercial code simulations (Fig. 3) exhibit an excellent agreement. Our interpretive transmission line approach (Fig. 4) produced a good agreement between the experimental data and simulations as well, especially when the wave was propagating along crystallographic directions such as $\langle 001 \rangle$ or $\langle 011 \rangle$. However, transmission line theory does not account for lateral mismatch between screens. The agreement between simulations and experimental data was made possible by introduction of a structural phase factor for each screen to account for its thickness and another phase factor to account for the lateral displacement between screens. Yet when the propagation is made along a more evolved crystallographic axis, such as along the $\langle 111 \rangle$ direction of cubic crystals, the simple picture of modes becomes too complex, owing to the large extent of mode mixing.

In summary, we have provided a simple way to interpret all transmission resonance in stacked, thick capacitive screens when propagation occurs along specific crystallographic axes.

APPENDIX A: TRANSMISSION LINE THEORY FOR A SUCCESSION OF SCREENS

Transmission line theory for the calculation of reflectance and transmittance of thin inductive and capacitive metal screens has been developed previously.[18] A short description is given in Ref. 16. The original scheme was later corrected[19] and will be used here with some modifications. We start with a simulation[15] of a single metallo-dielectric capacitive screen. The output of these simulations results in three parameters: the resonance frequency ω_0, the resonance bandwidth $\Delta\omega$, and the metal loss parameter α. A single screen is described by shunt impedance.[19] Therefore for a lattice constant g,

$$Y(\lambda) = 1/[\alpha + (i\Omega(\lambda)/2\omega_1 N \Delta\omega)]. \tag{A1}$$

Here

$$\Omega(\lambda) = g/\lambda\omega_0 - \lambda\omega_0/g, \tag{A2}$$

$$N = (n_1{}^2 + n_2{}^2). \tag{A3}$$

The wave propagates in a medium with refractive index n_1, and the corresponding value for the dielectric portion of the screen is n_2. The resonance frequency ω_0, its width $\Delta\omega$, and the loss parameter α, are all taken from the simulation of a single screen.

The single-screen simulations are followed by transmission line theory of stacked or cascaded screens.[20] The incident and reflected waves are related by a 2×2 matrix $\mathbf{M}$ to the transmitted and backward-traveling waves, $b_1 = m_{11}a_2 + m_{12}b_2$ and $a_1 = m_{21}a_2 + m_{22}b_2$. For $a_2 = 0$, that is, for the case with no backward-traveling wave, the ratio between the reflected wave b_1 and incident wave a_1 is $b_1/a_1 = m_{12}/m_{22}$. The ratio between the transmitted wave b_2 and the incident wave a_1 is $b_2/a_1 = 1/m_{22}$. The transmitted intensity is calculated from the (2, 2) element of the resulting matrix.

The matrix **MC** representing one layer has the elements

$$\mathrm{mc}_{11} = (-Y/2 + 1)\exp[-i\Phi(\lambda)], \qquad \mathrm{mc}_{12} = -Y/2,$$

$$\mathrm{mc}_{21} = Y/2, \qquad \mathrm{mc}_{22} = (Y/2 + 1)\exp[+i\Phi(\lambda)]. \tag{A4}$$

The matrix **MS** represents the propagation in between screens at separation s:

$$\mathrm{ms}_{11} = \exp[-i2\pi s\,\mathrm{n}_1/\lambda - i\Phi^{(s)}(\lambda)], \qquad \mathrm{ms}_{12} = 0, \tag{A5}$$

$$\mathrm{ms}_{21} = 0, \qquad \mathrm{ms}_{22} = \exp[i2\pi s\,\mathrm{n}_1/\lambda + i\Phi^{(s)}(\lambda)]. \tag{A6}$$

In a departure from the standard transmission line theory, we introduce a structural phase $\Phi(\lambda)$ to account for the screen thickness and to accommodate lattice parameters, which are more complex than for a typical cubic lattice.

A multilayer metallo-dielectric crystal is therefore represented by a product of matrices: $\mathbf{M} = [\mathbf{MC}] \times [\mathbf{MS}]\ldots[\mathbf{MC}]$. Thus for a cubic crystal we get

$$\mathbf{MC}(\lambda)_{\mathrm{cubic}} = [\mathbf{MC}(\lambda)\mathbf{MS}1(\lambda)]^f\mathbf{MC}(\lambda), \tag{A7}$$

where f is the number of layers plus 1 and $s1$ is the separation between the layers. As mentioned above, the input transverse resonance frequency ω_0 is taken from simulations for a single screen, and all refractive indices are set to unity. The phase is $\Phi(\lambda)_{\mathrm{cubic}} = \tan^{-1}[\lambda d/\pi n_2 W_{\mathrm{eff}}^2] + c_1$, where $2W_{\mathrm{eff}} = (a - d)/\sqrt{2}$ is the effective opening in the screen (formed by an equivalent circular opening), d is the metal sphere's diameter, a is the lattice constant, n_2 is the refractive index of the

screen's dielectric material, and $c_1 = (\sqrt{3})\pi/2$ is a phase constant independent of the wavelength. In addition, $\Phi^{(s)}_{\text{cubic}}(\lambda) = 0$. The BCC crystal is represented by

$$\mathbf{MC}(\lambda)_{\text{BCC}} = [\mathbf{MC}(\lambda)\mathbf{MS}2(\lambda)]^f\mathbf{MC}(\lambda), \qquad \text{(A8)}$$

where the separation s between screens is now one half of the value used for the cubic crystal. The transverse resonance frequency is the same for all screens. The phases for the BCC crystal are, for the individual screen,

$$\Phi(\lambda)_{\text{BCC}} = \tan^{-1}[\lambda d/\pi n_2 W^2_{\text{eff}}] + c_1 = \Phi(\lambda)_{\text{C}},$$

$$\Phi^{(s)}_{\text{BCC}}(\lambda) = c_1 = (\sqrt{3})\pi/2.$$

The results of the calculations are shown in Fig. 4.

ACKNOWLEDGMENT

This research was funded in part by National Science Foundation grant ECE9820200 and Army Research Office contract DAAD19-01-1-0009.

Corresponding author Haim Grebel's e-mail address is grebel@njit.edu.

REFERENCES

1. J. M. Tobias, M. Ajgaonkar, and H. Grebel, "Morphology-dependent transmission through photonic crystals," J. Opt. Soc. Am. B **19**, 385–391 (2002).
2. H. Grebel and J. Tobias, "Study of hybrid metal-dielectric photonic crystals," presented at the Quantum Electronics and Laser Science Conference, San Francisco, Calif., May 2002, paper QTuF1.
3. H. Grebel, Z. Iqbal, and A. Lan, "Detection of C_{60} using surface enhanced Raman scattering from metal coated periodic structures," Appl. Phys. Lett. **79**, 3194–3196 (2001).
4. J. M. Tobias and H. Grebel, "Self-imaging in photonic crystals in a subwavelength range," Opt. Lett. **24**, 1660–1662 (1999).
5. S. Vijayalakshmi, H. Grebel, G. Yaglioglu, R. Dorsinville, and C. W. White, "Nonlinear dispersion properties of subwavelength photonic crystals," Appl. Phys. Lett. **78**, 1754–1756 (2001).
6. A. Serpenguzel, "Transmission characteristics of metallodielectric photonic crystals and resonantors," IEEE Microwave Wireless Compon. Lett. **134**, 134–136 (2002).
7. J. S. McCalmont, M. M. Sigalas, G. Tuttle, K.-M. Ho, and C. M. Soukolis, "A layer-by-layer metallic photonic band-gap structure," Appl. Phys. Lett. **68**, 2759–2761 (1996).
8. J. G. Fleming, S. Y. Lin, I. El-Kady, R. Biswas, and K. M. Ho, "All metallic three-dimensional photonic crystals with a large infrared band-gap," Nature **417**, 52–55 (2002).
9. K. D. Möller, O. Sternberg, H. Grebel, and K. P. Stewart, "Near-field effects in multilayer inductive metal meshes," Appl. Opt. **41**, 1942–1948 (2002).
10. J. Li, L. Zhou, C. T. Chan, and P. Sheng, "Photonic band gap from a stack of positive and negative index materials," Phys. Rev. Lett. **90**, 083901-1–083901-4 (2003).
11. M. Born and E. Wolf, *Principles of Optics*, 2nd ed. (Pergamon, Oxford, UK, 1964).
12. K. D. Möller, O. Sternberg, H. Grebel, and P. Lalanne, "Thick inductive cross shaped metal meshes," J. Appl. Phys. **91**, 9461–1965 (2002).
13. L. Martin-Moreno, F. J. Garcia-Vidal, H. J. Lezec, K. M. Pellerin, T. Thio, J. B. Pendry, and T. W. Ebbesen, "Theory of extraordinary optical transmission through subwavelength hole arrays," Phys. Rev. Lett. **86**, 1114–1117 (2001).
14. O. Sternberg, "Resonances of periodic metal-dielectric meshes in the infrared wavelength region," Ph.D. thesis (New Jersey Institute of Technology, Newark N.J. 07102, 2002<).
15. "Micro-Stripes Program" by Flomerics, Inc., 275 Turnpike Road, Suite 100, Southborough, Mass., 01772.
16. K. D. Möller and W. G. Rothschild, *Far Infrared Spectroscopy* (Wiley, New York, 1971).
17. R. Ulrich, "Mode of propagation on an open periodic waveguide for far infrared," Microwave Symposia Series, Vol. XXIII (Polytechnique Press, Brooklyn, N.Y., 1974).
18. R. Ulrich, "Far-infrared properties of metallic mesh and its complementary structure," Infrared Phys. **7**, 37–55 (1967).
19. L. B. Whitbourn and R. C. Compton, "Equivalent-circuit formulas for metal grid reflectors at dielectric boundary," Appl. Opt. **24**, 217–220 (1985).
20. T. Timusk and P. L. Richards, "Near millimeter wave bandpass filters," Appl. Opt. **20**, 1355–1360 (1981).